Modulation of Protein Function by Exogenous Ligands in Protein Cavities: CO Binding to a Myoglobin Cavity Mutant Containing Unnatural Proximal Ligands†

Sean M. Decatur, Gia D. DePillis, and Steven G. Boxer*

Department of Chemistry, Stanford University, Stanford, California 94305-5080

Received November 6, 1995; Revised Manuscript Received January 18, 1996⊗

ABSTRACT: A variety of heterocyclic ligands can be exchanged into the proximal cavity of sperm whale myoglobin mutant H93G, providing a simple method for introduction of the equivalent of unnatural amino acid side chains into a functionally critical location in this protein. These modified proteins bind CO on the distal side. ^{1}H NMR data on H93G(Im)CO, where Im is imidazole, demonstrate that the structure of the distal heme pocket in H93G(Im)CO is very similar to that of wild type; thus, the effects of the proximal ligand's properties on CO binding can be studied with minimal perturbation of distal pocket structure. The exogenous proximal ligands used in this study include imidazole (Im), 4-methylimidazole (4-MeIm), 4-bromoimidazole (4-BrIm), *N*-methylimidazole (*N*-MeIm), pyridine (Pyr), and 3-fluoropyridine (3-FPyr). Substitution of the proximal ligand is found to produce substantial changes in the CO on and off rates, the equilibrium binding constant, and the vibrational stretch frequency of CO. Many of the changes are as large as those reported for distal pocket mutants prepared by site-directed mutagenesis. The ability to systematically vary the nature of the proximal ligand is exploited to test the effects of particular properties of the proximal ligand on CO binding. For example, 4-MeIm and 4-BrIm are similar in size and shape but differ significantly in pK_a. The same relationship is true for Pyr and 3-FPyr. By comparison of the IR spectra and CO recombination kinetics of these complexes, the effects of proximal ligand pK_a on the CO binding are assessed. Likewise, *N*-MeIm and 4-MeIm are similar in size and pK_a but differ in their ability to hydrogen bond to amino acid residues in the proximal cavity. Comparisons of IR spectra and CO binding kinetics in these complexes reveal that proximal ligand conformation and hydrogen bonding affect the kinetics of CO binding. The mechanism of proximal ligand exchange between solution and the proximal cavity in CO complexes was investigated by obtaining the ^{19}F NMR spectrum of H93G(3-FPyr)CO, whose ^{19}F signal can be observed without interference from resonances of the protein. The proximal ligand is found to exchange within a few seconds by saturation transfer. This exchange rate is about 2 orders of magnitude faster than what is observed for the isoelectronic metcyano complex [Decatur, S. M., & Boxer, S. G. (1995) *Biochemistry 34*, 2122−2129]; in both the ferrous CO and ferric cyano complexes, the proximal ligand exchange rate is independent of ligand concentration. These results suggest that the rate-limiting step in proximal ligand exchange is breakage of the iron−ligand bond, followed by rapid diffusion of the ligand through the protein to bulk solution.

The binding of diatomic ligands such as carbon monoxide (CO)[1] to myoglobin is the classic model for understanding protein structure−function relationships. There is now an extensive literature on synthetic biomimetic heme complexes and naturally occurring or engineered myoglobin mutants (Momenteau & Reed, 1994; Springer et al., 1994; Traylor & Traylor, 1982). Much of the effort on both model heme complexes and site-directed mutants of myoglobin and hemoglobin is directed toward understanding the interactions between diatomic ligands such as O_2, CO, and NO and the environment of the distal heme pocket (Collman et al., 1979; Nagai et al., 1987; Olson et al., 1988; Lambright et al., 1989, 1994; Egeberg et al., 1990; Balasubramanian et al., 1993a).

The role of the proximal side of the heme is less understood, though equally important. The proximal ligand has been varied extensively in synthetic heme models, demonstrating that properties of the proximal ligand such as pK_a (El-Kasmi, et al., 1995; Lavalette et al., 1995; Alben & Caughey, 1968) and strain (Rougee & Brault, 1975; Collman et al., 1978; Traylor et al., 1979) modulate iron−oxygen or iron−CO bonding. A few studies in globins also emphasize the importance of the proximal residue. For example, Perutz identified strain in the proximal histidine as a contributing factor to the reduced O_2 and CO affinities in T-state hemoglobin (Perutz, 1970). Mutation of Ser 92, which forms a weak hydrogen bond to proximal histidine 93 in pig (Smerdon et al., 1993) and human (Shiro et al., 1994) myoglobins, results in subtle changes in proximal ligand conformation and distal CO and O_2 binding affinities.

In contrast to the situation for simple heme model compounds, one of the difficulties in systematically varying the properties of the proximal ligand in Mb is the lack of

† This work is supported in part by Grant GM27738 from the National Institutes of Health. FTIR data were obtained using instrumentation provided by the Stanford Free Electron Laser Facility supported by the Office of Naval Research under Contract N00014-91-C-0170. S.M.D. was the recipient of an NSF Predoctoral Fellowship and a Ford Foundation Dissertation Fellowship. G.D.D. was the recipient of an NIH Postdoctoral Fellowship.

⊗ Abstract published in *Advance ACS Abstracts,* March 1, 1996.

[1] Abbreviations: CO, carbon monoxide; MbCO, carbon monoxy-myoglobin; WT, wild type; NMR, nuclear magnetic resonance; FTIR, Fourier transform infrared; H93G(L), H93G myoglobin with L as a proximal ligand; Im, imidazole; MeIm, methylimidazole; L, proximal ligand; Pyr, pyridine; 3-FPyr, 3-fluoropyridine.

0006-2960/96/0435-3925$12.00/0

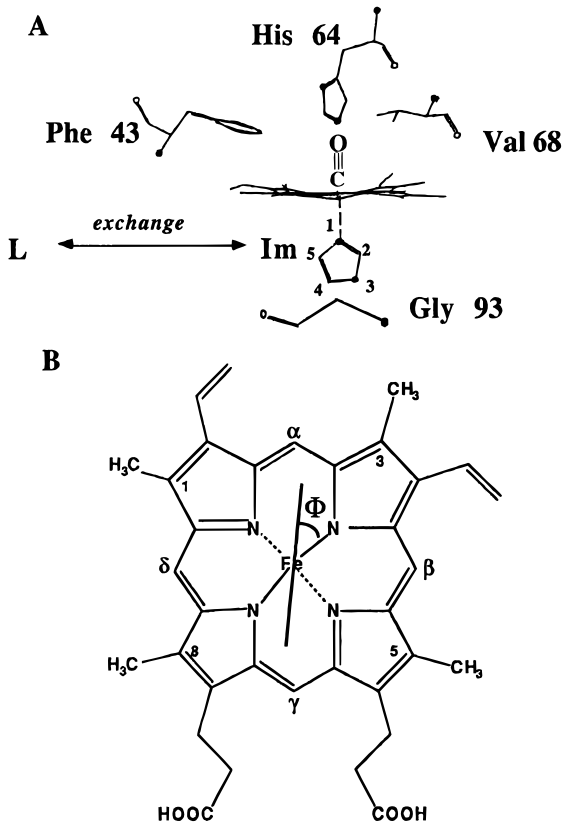

FIGURE 1: (A) Schematic diagram of the heme pocket in H93G(Im)CO, assuming it is the same as found for the metaquo form (Barrick, 1994). The proximal imidazole can be exchanged with many exogenous ligands (L) from solution (DePillis et al., 1994). (B) Projection of the Im plane onto the heme plane. The angle Φ between the Im projection and the $N_{IV}-Fe-N_{II}$ plane is about 10° in WT sperm whale Mb, with His 93 nearly eclipsing the heme pyrrolic nitrogens (Takano, 1977). In metH93G(Im), Φ is closer to 45°, and the Im projection is aligned with the $C_\alpha-C_\gamma$ meso carbons of the heme (Barrick, 1994).

heme ligands similar to histidine among the twenty naturally occurring amino acids. While large changes, such as proximal histidine 93 to cysteine or tyrosine, models for cytochrome P450 and catalase, respectively, have been made in several myoglobins (Egeberg et al., 1990; Adachi et al., 1993; Hildebrand et al., 1995), there are no naturally occurring amino acids which allow the subtle variation of proximal ligand properties. As illustrated in Figure 1A, exogenous imidazole (Im) can be specifically incorporated into the proximal cavity created by elimination of the histidine 93 side chain in the sperm whale myoglobin mutant H93G, and it serves as the fifth ligand to the heme iron (Barrick, 1994). In previous reports, we have demonstrated that this imidazole can be replaced with a wide range of heterocyclic ligands L, producing unique proteins denoted H93G(L) (DePillis et al., 1994) distinguishable by their ^{1}H NMR (Decatur & Boxer, 1995a) and electronic absorption spectra and CO recombination kinetics. In this paper, we report a detailed characterization of the CO complexes of these proteins via NMR and FTIR spectroscopies, as well as values for k_{on} and k_{off} of CO. The ability to systematically vary the nature of the proximal ligand is exploited to test the effects of particular properties of the proximal ligand on CO binding. In addition, information is obtained on the mechanism by which the exogenous ligand exchanges into the proximal cavity from bulk solution.

MATERIALS AND METHODS

Protein Preparation. The sperm whale myoglobin mutant H93G was expressed in *Escherichia coli* and purified as described in detail elsewhere (Barrick, 1994). The cavity mutant is purified with imidazole as the proximal ligand; this ligand can be exchanged for other ligands (L) via diafiltration (DePillis et al., 1994). The exogenous proximal ligands used in this study include imidazole (Im), 4-methylimidazole (4-MeIm), 4-bromoimidazole (4-BrIm), *N*-methylimidazole (*N*-MeIm), pyridine (Pyr), and 3-fluoropyridine (3-FPyr). Carbon monoxy complexes were formed by purging the samples with CO, followed by reduction with a minimum amount of freshly prepared 1 M sodium dithionite solution. Samples were then equilibrated with additional CO.

NMR Spectroscopy. ^{1}H NMR spectra were measured at 500 MHz on a GE Omega spectrometer. Samples contained about 3 mM protein in 0.1 M sodium phosphate/D_2O buffer, pH 7.0. For H93G(L) samples, 1 mM excess L was present in the solutions. For one-dimensional spectra, 2*K* data points were collected over a spectral window of 10 000 Hz. Spectra were acquired with presaturation at the residual H_2O peak. Assignments of protons of the heme and of some amino acids of the heme pocket were made using COSY and NOESY data, following the methods of Dalvit and Wright (1987). All data analysis was performed using the program FTNMR (Hare Research).

^{19}F NMR spectra were collected at 470 MHz on the Omega spectrometer using an ^{1}H probe modified for optimal collection of ^{19}F data (Fremont Magnetic Resonance, Fremont, CA). Chemical shifts were referenced to trifluoroacetic acid via the free 3-FPyr resonance. Saturation transfer was measured using standard pulse sequences (Alger & Shulman, 1984). Briefly, spectra were collected with the decoupler channel tuned alternately on- and off-resonance with the free ligand resonance. The saturation time was greater than $T_{1free} + k_{exch}^{-1}$, and the relaxation time between acquisitions was $7T_{1bound}$. Typically, 1000 scans of 4096 points were collected over a spectral window of 10 000 Hz. Data were apodized by an exponential function with a line-broadening factor of 3 Hz. T_1 values for bound 3-FPyr were determined by standard $180°-\tau-90°$ inversion recovery experiments with the free 3-FPyr resonance saturated at all times except during acquisition to eliminate chemical exchange effects (Alger & Schulman, 1984; Mann, 1977).

FTIR Spectroscopy. FTIR spectra were measured on a Bruker ISF113 spectrometer. The concentration of the protein samples was ~5 mM in 0.1 M sodium phosphate/D_2O buffer, pH 7.0. The protein solution was reduced by addition of a minimum volume of freshly prepared 1 M sodium dithionite solution, equilibrated with CO, and loaded into a purged, sealed solution cell composed of $CaFl_2$ windows separated by a 100 μm lead spacer. Spectra were measured at room temperature in an N_2-purged sample well. A blank sample of D_2O buffer was used to correct for solvent absorption.

Measurement of k_{on}. CO recombination rates were measured by flash photolysis as described elsewhere (Lambright et al., 1989, 1994). For the complexes presented here, the final phase of CO recombination is the only phase which

Table 1: Assignments of Selected Protons of the Heme and of Heme Pocket Amino Acids

proton	WT MbCO[a]	H93G(Im)CO	H93G(Pyr)CO
Val 68 CγH$_3$	−2.3	−2.3	−2.3
CγH$_3$	−0.55	−0.5	−0.5
C$_{\beta H}$	0.84	1.0	1.0
heme α-meso H	9.92	10.07	10.13
β-meso H	9.34	9.27	9.38
γ-meso H	10.15	10.35	10.44
δ-meso H	9.86	9.73	9.70
1-methyl	3.63	3.67	3.65
3-methyl	3.79	3.86	3.85
5-methyl	2.53	2.53	2.53
8-methyl	3.59	3.52	3.58
2-vinyl α	8.43	8.64	8.70
4-vinyl α	8.62	8.52	8.55

[a] Mabbut and Wright (1985) and Dalvit and Wright (1987).

depends on CO concentration and corresponds to bimolecular recombination (Balasubramanian et al., 1993b; G. D. DePillis and S. G. Boxer, unpublished results). Under the conditions of this experiment, the rate of bimolecular CO recombination is pseudo-first order; values of k_{on} were determined from a fit of this phase to a single exponential.

Measurement of k_{off}. CO dissociation rates were measured using the NO replacement method (Gibson & Roughton, 1957; Lambright et al., 1989). Concentrated stocks of Mb were purged with N_2, equilibrated with CO, and reduced with sodium dithionite. Approximately 3 mL of 0.1 M phosphate buffer, pH 7.0, was added to a sealed 1 cm path length cuvette; the buffer was deoxygenated by purging with N_2 for 15 min and then saturated with NO. The concentrated protein stocks (10 μL) were diluted into the NO buffer ([MbCO] $\approx$ 5 μM). The replacement of CO by NO following thermal dissociation of H93G(L)CO can be described by the following scheme:

$$\underset{\lambda_{max}^{Soret} = 423\ nm}{H93G(L)CO} \xrightarrow{k_{off}} H93G(L) + NO \xrightarrow{fast}$$

$$H93G(L)NO \xrightarrow{fast} \underset{\lambda_{max}^{Soret} = 400\ nm}{H93G{-}NO} + L$$

In contrast to WT Mb, NO binding to H93G(L) results in rapid release of the proximal ligand and rapid formation of a stable five-coordinate NO heme complex H93G-NO under the conditions of this experiment (Decatur et al., 1995). Thus, the dissociation of CO from H93G(L)CO is monitored by the decay of the absorbance at 423 nm. The decays were fit by a single exponential using a nonlinear least squares method.

RESULTS

^{1}H NMR Characterization of H93G(Im)CO. Overall, the features of the H93G(Im)CO spectrum are very similar to those of wild type, demonstrating that the protein is a well-defined diamagnetic complex. Assignments of selected protons of the heme and heme pocket amino acids are listed in Table 1. The assignment process followed that used by Wright and co-workers for the assignment of WT MbCO (Mabutt & Wright, 1985; Dalvit & Wright, 1987); details are given in the supporting information. One of the few readily observed protein protons in the one dimensional ^{1}H NMR spectrum of MbCO is the isolated upfield-shifted

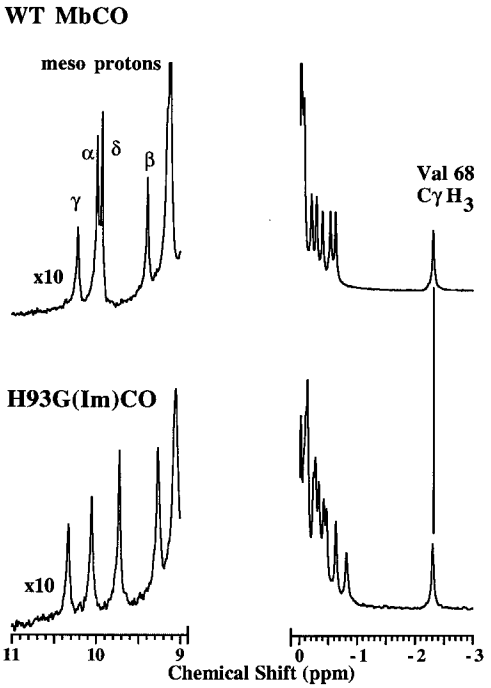

FIGURE 2: Upfield region of the ^{1}H NMR spectra of WT MbCO and H93G(Im)CO, pH 7.0, at 30 °C showing the resonance for Val 68 CγH$_3$ protons at −2.30 ppm.

methyl resonance of Val 68 CγH$_3$ at −2.30 ppm (*cf.* Figure 1B). The chemical shift for Val CγH$_3$ is identical in WT and H93G(Im)CO as shown in Figure 2. Some resonances of the heme protons can be assigned on the basis of NOESY spectra as described by Mabbutt and Wright (1985). Overall, the chemical shifts of the heme meso protons of H93G(Im)-CO and WT MbCO are very similar, with large upfield shifts relative to free heme observed for the β-meso and 5-methyl protons due to the proximity of Phe 43 (*cf.* Figure 1B). Some subtle differences between H93G(Im)CO and WT MbCO are observed for the heme meso proton resonances (Figure 2 and Table 1). These changes are likely due to the differences in the conformation of the proximal imidazole ring in H93G and wild type, as schematically diagrammed in Figure 1B and discussed below. As shown in Table 1, all of the differences between WT MbCO and H93G(Im)-CO are also observed when pyridine replaces imidazole as the proximal ligand, while the positions of the distal Val 68 CγH$_3$ protons remain identical.

^{19}F NMR Spectra of H93G(3-FPyr)CO. Introduction of fluorinated ligands into H93G allows the observation of ligand ^{19}F resonances without interference or congestion from protein signals. A spectrum of H93G(3-FPyr)CO is shown in Figure 3; the resonance from 3-fluropyridine (3-FPyr) bound to the protein is shifted upfield from that of free 3-FPyr by about 4 ppm, as expected given the large ring current of the heme. The resonance from free 3-FPyr is sharper with a longer T_1 value (1.5 s) than the resonance from the bound species (0.57 s). A minor peak is also observed upfield from the major 3-FPyr resonance with an area of ~10% of the bound peak.

Upon addition of an excess of 3-FPyr to H93G(Im)CO, the bound ^{19}F resonance appears within the minimum time required to obtain a spectrum (about 1 min; data not shown); thus, the 3-FPyr is in rapid equilibrium between free and

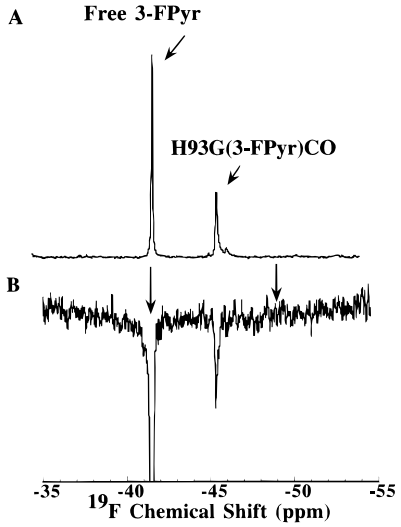

FIGURE 3: (A) ^{19}F NMR spectrum of H93G(3-FPyr)CO, pH 7.0, 40 at °C. (B) Difference spectrum, on-resonance minus off-resonance, upon saturation of the free 3-FPyr resonance. Chemical shifts are relative to trifluoroacetic acid.

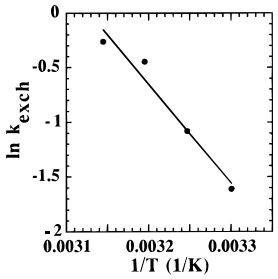

FIGURE 4: Arrhenius plot of k_{exch} for 3-FPyr in H93G(3-FPyr)CO determined from saturation transfer experiments (*cf.* Figure 3B). The points can be fit with a line to give an activation energy E_a = 75 kJ/mol and prefactor $A = 1.8 \times 10^{12}$.

bound states:

$$\text{bound 3-FPyr} \overset{k_{exch}}{\rightleftharpoons} \text{free 3-FPyr} \qquad (1)$$

The rate of exchange of 3-FPyr in and out of the protein cavity was measured by saturation transfer. If the rate of exchange between free and bound states is on the order of the spin−lattice relaxation time (T_1) for the fluorine nucleus, transfer of magnetization from free to bound ligand can occur. Upon saturation of the free 3-FPyr resonance, the fraction of saturation transfer ($\Delta M_{bound}/M_{bound}$) to the bound 3-FPyr resonance is related to the first order rate constant k_{exch} by eq 2 (Alger & Shulman, 1984):

$$k_{exch} = \frac{\left(\frac{\Delta M_{bound}}{M_{bound}}\right)\left(\frac{1}{T_{1bound}}\right)}{1 - \frac{\Delta M_{bound}}{M_{bound}}} \qquad (2)$$

A difference spectrum following saturation on- and off-resonance with free 3-FPyr contains a negative peak at the resonance for bound 3-FPyr (Figure 3B). By application of eq 2, k_{exch} is calculated to be 0.23 ± 0.03 s^{-1} at 30 °C, or $\tau_{exch} \sim 4$ s. Upon variation of the temperature in the range 30°−45 °C, k_{exch} exhibits Arrhenius behavior (Figure 4). The NMR spectra were similar throughout the temperature range, and thus, the myoglobin sample maintains its integrity at

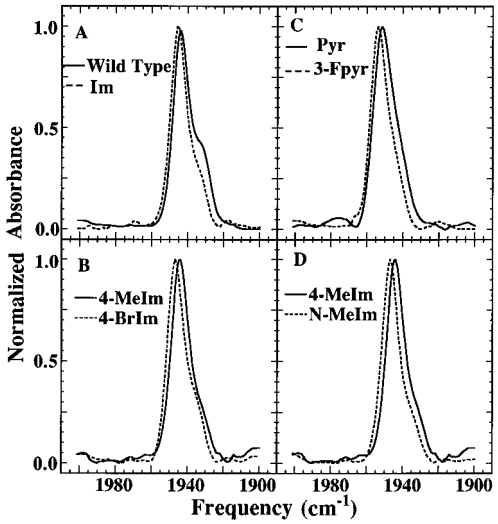

FIGURE 5: FTIR spectra of (A) H93G(Im)CO and WT MbCO, (B) H93G(4-MeIm)CO and H93G(4-BrIm)CO, (C) H93G(Pyr)CO and H93G(3-FPyr)CO, and (D) H93G(4-MeIm)CO and H93G(N-MeIm)CO. All spectra were recorded at room temperature in pH 7.0 phosphate buffer prepared in D_2O. Data are summarized in the last column of Table 2.

temperatures as high as 45 °C. The data can be fit to give an activation energy E_a = 75 kJ/mol and prefactor $A = 1.8 \times 10^{12}$. The rate of ligand exchange was found to be independent of the concentration of free 3-FPyr (data not shown), indicating that the rate-limiting step in proximal ligand exchange is a unimolecular process. We obtained a similar result for Im and several methyl-substituted imidazoles in H93G(Im)CN (Decatur & Boxer, 1995a); however, the rate for proximal ligand exchange in the metcyano complexes is about 2 orders of magnitude slower than in the CO complexes observed here.

FTIR spectra of H93G(L)CO. The FTIR spectra of H93G(Im)CO and WT MbCO in the region of the CO stretch mode are compared in Figure 5A. At room temperature and pH 7.0, the IR spectrum of sperm whale myoglobin is dominated by bands at 1945 and 1933 cm^{-1}, referred to as A_1 and A_3, respectively (Alben et al., 1982). In H93G(Im)CO, the A_3 band has a significantly smaller amplitude, apparent as only a small shoulder on A_1; this is also observed in other H93G(L)CO spectra (Figure 5B−D). ν_{CO} varies in H93G(L)CO as the properties of L are changed, as summarized in Table 2. Two trends are apparent in the data. As the solution pK_a of the ligands decreases (see Table 2), while size, shape, and conformation are held constant (for example, 4-MeIm and 4-BrIm or Pyr and 3-FPyr), ν_{CO} increases (Figure 5B, C). Interestingly, *N*-MeIm and 4-MeIm also have different ν_{CO} values (Figure 5D), although their solution pK_a values are very similar. This difference in A_1 frequency likely reflects the influence of hydrogen bonding between the proximal ligand and neighboring amino acid residues on Fe−CO bonding.

Kinetic and Equilibrium CO Binding. The k_{on} for CO binding to H93G(L) was measured using flash photolysis; sample data are given in Figure 6, and the rate constants are summarized in Table 2. As with ν_{CO}, there are systematic variations in k_{on} with changes in L. As the solution pK_a of L is changed while the size and shape of L are kept the same (4-MeIm vs 4-BrIm or Pyr vs 3-FPyr), k_{on} increases with decreasing pK_a (Figure 6A,B). The k_{on} of *N*-MeIm is

Table 2: Properties of H93G(L)CO Complexes, Measured at 23 °C

ligand	pK_a	k_{on} ($\times 10^{-6}$ M^{-1} s^{-1})	k_{off} ($\times 10^{-2}$ s^{-1})	k_{on}/k_{off} ($\times 10^{-6}$ M^{-1})	ν_{CO} (cm^{-1})
wild type	–	0.77	2.2	34	1944
imidazole	6.9[a]	1.7	1.1	141	1945
4-methylimidazole	7.5[a]	1.2	1.4	86	1944
4-bromoimidazole	3.6[a]	2.0	1.2	167	1947
N-methylimidazole	7.2[a]	4.3	0.77	558	1947
pyridine	5.2[b]	2.3	6.5	35	1951
3-fluoropyridine	3.0[b]	3.9	5.8	67	1953

[a] Taken from Hofmann (1953). [b] From Mertel (1961).

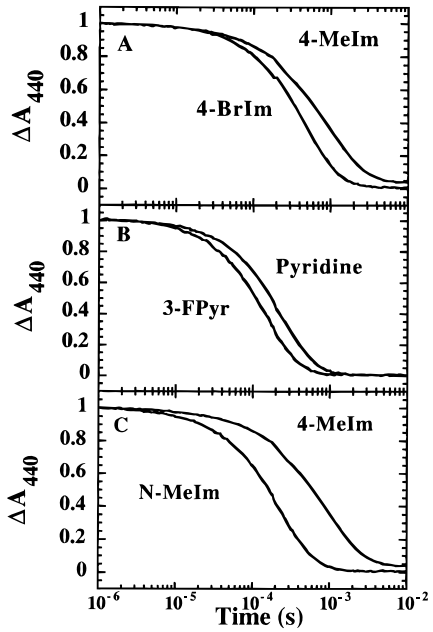

FIGURE 6: CO recombination upon flash photolysis for (A) H93G-(4-MeIm)CO and H93G(4-BrIm)CO, (B) H93G(Pyr)CO and H93G-(3-FPyr)CO, and (C) H93G(N-MeIm) and H93G(4-MeIm). All data were recorded in pH 7.0 phosphate buffer, 1 atm of CO, at room temperature. Data are normalized at the beginning of the bimolecular phase of recombination (1 μs) to facilitate comparison and are shown as progress curves vs log time. Rate constants k_{on} were determined from a single exponential fit and are summarized in Table 2.

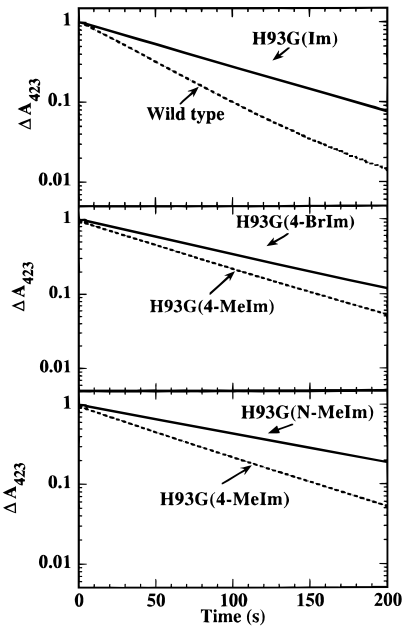

FIGURE 7: Measurement of k_{off} for H93G(L)CO by the NO replacement method. Measurements were made at room temperature and pH 7.0. Rate constants k_{off} were determined from a single exponential fit and are summarized in Table 2. The raw data are shown.

significantly faster than that of 4-MeIm, even though the solution pK_a values of these two ligands are comparable (Figure 6C).

The CO dissociation rate constant k_{off} also varies with changes in proximal ligand (Figure 7). Decreasing the solution pK_a (4-MeIm vs 4-BrIm or 3-FPyr vs Pyr) results in a modest decrease in k_{off}. Larger changes in k_{off} occur upon changing the conformation or size of the ligand, such as in *N*-MeIm compared with 4-MeIm. The changes in both k_{on} and k_{off} result in substantial changes in the apparent equilibrium constant, $K_{CO} = k_{on}/k_{off}$ (Table 2).

DISCUSSION

Structural Features of H93G(L)CO. The H93G(Im) complex has been characterized in the metaquo form by X-ray crystallography (Barrick, 1994) and in the metcyano form by ^{1}H NMR spectroscopy (Decatur & Boxer, 1995a). In those studies, the Im was shown to bind specifically in the proximal cavity, with the overall structure of the distal pocket remaining the same as in the wild type protein. The ^{1}H NMR spectrum of H93G(Im)CO indicates that this is also true in the carbon monoxy complex. In particular, the chemical shifts of the protons of distal pocket residue Val 68 are the same in WT and H93G(Im)CO. The ring current-shifted resonance of Val 68 CγH$_3$ is particularly sensitive to changes in the distal pocket structure; small adjustments of Val 68 conformation can result in sizable changes in its chemical shift, as seen in the spectra of proteins with modified or protonated distal histidines (Adachi & Morishima, 1992; S. M. Decatur and S. G. Boxer, unpublished results). Thus, the fact that the Val 68 CγH$_3$ resonance is the same in H93G(Im)CO and WT indicates that the distal pocket structure of the mutant is similar to that of WT and that the Im binds in the proximal cavity, not on the distal side. In principle, the imidazole can also bind to the distal side of the heme, though this requires a large excess of imidazole for the wild type protein. When imidazole binds to the distal side of wild type Mb to form a diamagnetic ferrous MbIm complex, a shift of over 1 ppm occurs in the Val 68 CγH$_3$ resonance due to structural reorganization of the distal pocket to accommodate such a large distal ligand and the ring current from the bound imidazole (S. M. Decatur and S. G. Boxer, unpublished results). Because no such shift is seen in H93G(Im)CO, we conclude that the exogenous imidazole, when present in a slight excess, binds uniquely in the proximal cavity, as demonstrated in the X-ray crystal structure of metH93G(Im) (Barrick, 1994) and in NMR studies of H93G(Im)CN (Decatur & Boxer, 1995a).

The resonances of heme protons are also useful for gaining insight into the structure of the heme pocket in H93G(Im)-CO. While there are some small changes in chemical shift, the overall features of the heme proton resonances are quite similar. For example, the heme 5-methyl and β-meso protons experience significant upfield shifts relative to their solution values due to the proximity of Phe 43 on the distal side of the heme pocket (Table 2; Mabbutt & Wright, 1985). This is further evidence that neither the H93G mutation nor the proximal ligand exchange process introduces a significant perturbation to the distal pocket structure. Subtle changes are observed in the chemical shifts of the heme meso protons (Table 1). These shifts can be understood in terms of the differences in Im ring conformation between WT and H93G-(Im), illustrated in Figure 1B. When the Im plane is nearly aligned with the Cα−Cγ meso axis, the α and γ meso protons are close to the plane of the Im ring and therefore are deshielded due to the imidazole ring current. This results in a small downfield shift in the resonances of the α and γ meso protons, as seen in H93G(Im)CO compared to WT MbCO. Thus, the chemical shift differences of the α and γ meso protons between WT MbCO and H93G(Im)CO are consistent with the rotation of the Im ring plane relative to H93 seen in the X-ray structure of the metaquo form (Barrick, 1994) and the NMR spectrum of the metcyano complex (Decatur & Boxer, 1995a).

When the proximal imidazole is exchanged for pyridine, the resonance of Val 68 CγH$_3$ remains unchanged (Table 1), demonstrating again that the proximal ligand exchange process leaves the distal pocket structure intact. This is consistent with previous studies in the metcyano complex of H93G (Decatur & Boxer, 1995a). There are, however, some small differences between H93G(Im)CO and H93G-(Pyr)CO in the meso proton region. In H93G(Pyr)CO, the downfield shifts of the α and γ meso protons are slightly larger than in H93G(Im)CO. This may reflect the larger ring current for Pyr compared to that for Im.

The ^{19}F NMR spectrum of H93G(3-FPyr)CO contains one major resonance corresponding to bound 3-FPyr, which is shifted upfield from the resonance of free 3-FPyr by the large ring current of the heme (Figure 3). The minor resonance shifted 0.7 ppm from the major resonance could result from the presence of a small population of hemes rotated 180° about the meso Cα−Cγ axis, as characterized in MbCN by La Mar and co-workers (La Mar et al., 1989; Hauksson et al., 1990), or it could come from a small population of 3-FPyr with Φ 180° from the dominant value (*cf.* Figure 1B). In the case of Im, there is a strong hydrogen bond between the Im NH and Ser 92 which will reinforce the angle Φ; this interaction is absent in 3-FPyr.

Mechanism of Ligand Exchange in H93G(L)CO. In earlier work (Decatur & Boxer, 1995a), we reported the exchange kinetics of bound proximal ligands in the metcyano complexes of H93G. In those complexes, the rate of ligand exchange is very slow, with $\tau_{exch} \sim 6 \times 10^2$ s. In the experiments presented here on the CO complex, the proximal ligand exchanges with $\tau_{exch} \sim 4$ s, about 2 orders of magnitude smaller. Furthermore, in both cases, the exchange rate is independent of the concentration of external ligand. Two possible limiting mechanisms could explain the independence of the exchange rate on the concentration of free ligand. (i) The rate-determining step is iron−ligand bond breaking, and the exchange rate corresponds to k_{off} for the proximal ligand; or (ii) the rate-determining step is ligand entry or exit coupled with motion of the protein, while bond breakage and formation occur rapidly. Changing the oxidation state of the iron and the nature of the trans ligand should have minimal effect on the protein dynamics affecting ligand entry and exit, especially as H93G(Im)CO and metH93G-(Im)CN are isoelectronic and have similar heme pocket structures based on the ^{1}H NMR data present above. However, the ferric iron should have a much stronger affinity for the axial base than the ferrous species, so a change in oxidation state should significantly alter the kinetics of bond breakage. Because the kinetics of proximal ligand exchange are substantially faster in the carbon monoxy complex than in the metcyano complex, we conclude that the rate-determining step in the proximal ligand exchange process is cleavage of the proximal ligand−iron bond, followed by relatively more rapid diffusion of the ligand in and out of the protein.

If this mechanism is correct, the measured activation barrier for ligand exchange (75 kJ/mol, Figure 4) corresponds to the activation barrier to breaking the Fe−3-FPyr bond. The barrier for entry and exit of the ligand from the proximal cavity must be lower than this value. There have been few studies of the kinetics of the entry or exit of a medium-sized molecule from a buried cavity within a protein. The best-studied example is the entry and exit of distal pocket ligands in myoglobin, where the activation barrier to ligand escape has been measured experimentally (Lambright et al., 1994; Chatfield et al., 1990), as well as calculated from molecular dynamics simulations (Case & Karplus, 1979). The escape of *tert*-butyl isocyanide (comparable in size to fluoropyridine) has an activation barrier of about 34 kJ/mol (Chatfield et al., 1990). While the distal pocket is likely more flexible than the proximal cavity in H93G, these data are consistent with a lower barrier for ligand entry and exit than what we observe for the rate-limiting step in ligand exchange for H93G(3-FPyr). The central result is that rather large organic molecules can move between a buried site roughly 10 Å from the protein surface and solution on a time scale faster than a few seconds. Further study of ligand exchange kinetics in H93G Mbs with other distal ligands (for example, nitric oxide where the proximal ligand−Fe bond is broken, Decatur et al., 1995) is warranted as this exchange process may ultimately limit the utility of the functional cavity approach in this and other proteins.

Proximal Ligand Effects on ν_{CO}. The effects of distal pocket mutations on ν_{CO} have been well-documented (Balasubramanian et al., 1993; Li et al., 1993; Decatur & Boxer, 1995b). The results presented here demonstrate that the proximal ligand also plays a role in the determination of ν_{CO} and the heterogeneity of the spectrum. In all of the H93G-(L)CO spectra, the A_3 band is much smaller than the A_3 in wild type sperm whale MbCO. Since the structure of the distal pocket is not significantly changed in H93G(L)CO, the reduction of the A_3 band must arise from changes in the conformation of the proximal ligand relative to the histidine ring in wild type, such as the difference in angle Φ described in Figure 1B or differences in the tilt of the Im plane from the heme normal (Barrick, 1994). Changes in the A_3 amplitude have also been observed in the IR spectra of the SW Mb proximal pocket mutants L89I and H97F (Abadan et al., 1995). Interestingly, myoglobins from other species, including the human and horse proteins, lack the A_3 band

altogether (Balasubramanian et al., 1993a; S. M. Decatur and S. G. Boxer, unpublished observations**)**. The results from the H93G studies thus suggest that differences in the amplitude of A_3 among various myoglobins might arise from differences in the imidazole ring conformations. Consistent with this proposal, results from a recent *ab initio* study revealed large changes in Fe−CO bonding characteristics upon variation in the proximal histidine ring conformation (Jewsbury et al., 1994, 1995; Jewsbury & Kitagawa, 1995). Thus, a systematic correlation between iron−CO bonding and proximal ligand conformation may exist, and it may be possible to characterize this correlation quantitatively using the functional cavity approach. Such an effort is currently underway.

Variations in the solution pK_a of the proximal ligand result in small but systematic shifts in ν_{CO}. For example, H93G-(4-BrIm)CO has ν_{CO} shifted 2 cm^{-1} to lower energy from that of H93G(4-MeIm)CO; there is a similar difference between H93G(Pyr)CO and H93G(3-FPyr)CO. These shifts are consistent with a simple model of iron−CO π back-bonding. In π bonding between the iron and the CO, the iron donates electrons from d_{xz} and d_{yz} orbitals into π^* orbitals of the CO (Douglas et al., 1983). As electron density at the iron increases, the amount of iron → CO π bond donation increases, resulting in a decrease in CO bond order and ν_{CO}. Conversely, as the pK_a of the proximal ligand increases, there is less electron density on the iron available for π back-bonding with the CO, and the CO bond order and stretch frequency increase. Similar trends have been observed in model heme complexes (Alben & Caughey, 1968).

Proximal Ligand Effects on the Kinetics of CO Binding. Substitution of the proximal ligand also results in complexes with unique CO binding behavior. As the pK_a of the proximal ligand is increased, there is a small decrease in CO binding affinity, mostly due to a decrease in k_{on}. Similar effects have been noted in model hemes (Lavalette et al., 1995; El-Kasmi et al., 1995). At first, these results seem to contradict the observations from the FTIR spectra, where we argue that π back-bonding between the CO and the iron increases with pK_a of the proximal ligand because an increase in π back-bonding is generally associated with a stronger Fe−CO bond. However, the strength of the Fe−CO bond and the kinetics of CO binding also depend on σ bonding interactions. Proximal ligands with higher pK_a values are better σ donors and increase the electron density at the heme iron. The electrons of CO experience more repulsion from the electron-rich iron, and therefore, the barrier for CO binding increases (i.e., a decrease in the rate constant k_{on}) (Case et al., 1979; El-Kasmi et al., 1995). Thus, even when the amount of π bonding between the iron and the CO increases as shown by the FTIR results, the overall effect is a weaker CO affinity.

Proximal Ligand−Protein Interactions Modulate CO Binding. *N*-MeIm has a pK_a similar to that of 4-MeIm (7.5 compared to 7.2), but H93G(*N*-MeIm)CO has a ν_{CO} shifted to higher energy, an increased k_{on}, and a decreased k_{off} relative to H93G(4-MeIm)CO, resulting in a K_{CO} that is 5 times larger than that of H93G(4-MeIm)CO (Table 2). Unlike Im and 4-MeIm, *N*-MeIm cannot hydrogen bond with amino acids of the proximal pocket such as Ser 92 (Decatur & Boxer, 1995a; Decatur et al., manuscript in preparation). The X-ray structure of metaquo H93G(Im) shows that the Im ring is rotated (*cf.* Figure 1B) and tilted to bring the Im NH group closer to Ser 92 (Barrick, 1994) which should lead to a stronger hydrogen bond than in WT. Hydrogen bonding increases the anionic character of imidazole ligands. For example, model hemes with hydrogen-bonded imidazoles as axial ligands have spectroscopic and catalytic properties consistent with increased electron donation from the ligand to the iron, similar to hemes with an imidazolate anion as the proximal ligand. In this sense, the effective pK_a of a hydrogen-bonded imidazole ligand is greater than that of its non-hydrogen-bonded counterpart (Mincey & Traylor, 1979; Quinn et al., 1984; Traylor & Popovitz-Biro, 1988). Thus, one would expect the effective pK_a of *N*-MeIm, which is not hydrogen-bonded within the proximal cavity, to be lower than that of 4-MeIm or Im, which can participate in hydrogen bonding interactions. The IR data (shift of ν_{CO} to higher energy) and the CO binding data (faster k_{on} and slower k_{off}) are consistent with this picture of a significantly lower effective pK_a within the proximal cavity for *N*-MeIm than for 4-MeIm. This demonstrates the importance of the environment of the proximal heme pocket in modulation of CO binding properties.

Smerdon and co-workers have measured a small difference in CO recombination kinetics in the pig myoglobin mutant S92A, where the hydrogen bond between the proximal histidine and Ser 92 is removed (Smerdon et al., 1993), though the changes are smaller than those observed by replacement of 4-MeIm with *N*-MeIm in H93G. This might be because the histidine in wild type myoglobin hydrogen bonds with both Ser 92 and the backbone carbonyl of Leu 89 (Cheng & Shoenborn, 1991). Loss of the Ser 92 hydrogen bond still leaves the Leu 89 hydrogen bond in place; however, replacement of 4-MeIm by *N*-MeIm eliminates all possible hydrogen bonding interactions. Data on the double mutants H93G/S92A will be presented elsewhere (Decatur et al., manuscript in preparation).

SUPPORTING INFORMATION AVAILABLE

Two figures (examples of two-dimensional NMR spectra used to assign heme and heme pocket amino acid resonances) (3 pages). Ordering information is given on any current masthead page.

REFERENCES

Abadan, Y., Chien, E. Y. T., Chu, K., Eng, C. D., Nienhaus, U., & Sligar, S. G. (1995) *Biophys. J. 68,* 2495−2502.

Adachi, S.-I. and Morishima, I. (1992) *Biochemistry 31,* 8613−8618.

Adachi, S.-I., Nagano, S., Ishimori, K., Watanabe, Y., Morishima, I., Egawa, T., Kitagawa, T., & Makino, R. (1993) *Biochemistry 32,* 241−252.

Alben, J. O., & Caughey, W. S. (1968) *Biochemistry 7,* 175−183.

Alger, J. R., & Shulman, R. G. (1984) *Q. Rev. Biophys. 17,* 83−124.

Balasubramanian, S., Lambright, D. G., & Boxer, S. G. (1993a) *Proc. Natl. Acad. Sci. U.S.A. 90,* 4718−4722.

Balasubramanian, S., Lambright, D. G., & Boxer, S. G. (1993b) *Biochemistry 32,* 2202−2212.

Barrick, D. (1994) *Biochemistry 33,* 6546−6554.

Case, D. A., & Karplus, M. (1979) *J. Mol. Biol. 132,* 343−368.

Case, D. A., Huynh, B. H., & Karplus, M. (1979) *J. Am. Chem. Soc. 101,* 4433−4453.

Chatfield, M. D., Walda, K. N., & Magde, D. (1990) *J. Am. Chem. Soc. 112,* 4680−4687.

Collman, J. P., Brauman, J. I., Doxsee, K. M., Halbert, T. R., & Suslick, K. S. (1978) *Proc. Natl. Acad. Sci. U.S.A. 75*, 564−568.
Collman, J. P., Brauman, J. I., & Doxsee, K. M. (1979) *Proc. Natl. Acad. Sci. U.S.A. 76*, 6035−6039.
Cross, K. J. & Wright, P. E. (1985) *J. Magn. Reson. 64*, 220−231.
Dalvit, C. & Wright, P. E. (1987) *J. Mol. Biol. 194*, 313−327.
Decatur, S. M., & Boxer, S. G. (1995a) *Biochemistry 34*, 2122−2129.
Decatur, S. M., & Boxer, S. G. (1995b) *Biochim. Biophys. Res. Commun. 212*, 159−164.
Decatur, S. M., Franzen, S., DePillis, G. D., Dyer, R. B., Woodruff, W. H., & Boxer, S. G. (1996) *Biochemistry* (in press).
DePillis, G. D., Decatur, S. M., Barrick, D., & Boxer, S. G. (1994) *J. Am. Chem. Soc. 116*, 6981−6982.
Egeberg, K. D., Springer, B. A., Sliger, S. G., Carver, T. E., Rohlfs, R. J., & Olson, J. S. (1990) *J. Biol. Chem. 265*, 11788−11795.
El-Kasmi, D., Tetreau, C., Lavalette, D., & Momenteau, M. (1995) *J. Am. Chem. Soc. 117*, 6041−6047.
Hauksson, J. B., La Mar, G. N., Pande, U., Pandey, R. K., Parish, D. W., Singh, J. P., & Smith, K. M. (1990) *Biochim. Biophys. Acta 1041*, 186−194.
Hildebrand, D. P., Burk, D. L., Maurus, R., Ferrer, J. C., Brayer, G. D., & Mauk, A. G. (1995) *Biochemistry 34*, 1997−2005.
Hofmann, K. (1953) *Imidazole and Its Derivatives, Part 1*. Interscience Publishers, New York.
Jewsbury, P., & Kitagawa, T. (1995) *Biophys. J. 68*, 1283−1294.
Jewsbury, P., Yamamoto, S., Minato, T., Saito, M., & Kitagawa, T. (1994) *J. Am. Chem. Soc. 116*, 11586−11587.
Jewsbury, P., Yamamoto, S., Minato, T., Saito, M., & Kitagawa, T. (1995) *J. Phys. Chem. 99*, 12677−12685.
Kendrew, J. C. (1962) *Brookhaven Symp. Biol. 15*, 216−227.
La Mar, G. N., Pande, U., Hauksson, J. B., Pandey, R. K., & Smith, K. M. (1989) *J. Am. Chem. Soc. 111*, 485−491.
Lambright, D. G., Balasubramanian, S., & Boxer, S. G. (1989) *J. Mol. Biol. 207*, 289−299.
Lambright, D. G., Balasubramanian, S., Decatur, S. M., & Boxer, S. G. (1994) *Biochemistry 33*, 5518−5525.
Lavalette, D., El-Kasmi, D., Momenteau, M., & Teatreau, C. (1995) *Biophys. J. 68*, A236.
Li, T., Quillin, M. L., Phillips, G. N., Jr., & Olson, J. S. (1994) *Biochemistry 33*, 1433−1446.
Mabbutt, B. C., & Wright, P. E. (1985) *Biochim. Biophys. Acta 832*, 175−185.
Mann, B. E. (1977) *J. Magn. Reson. 725*, 91−94.
Mertel, H. M. (1961) in *Pyridine and Its Derivatives, Part 2* (Klingsberg, E., Ed.) pp 299−419, Interscience Publishers, New York.
Mincey, T., & Traylor, T. G. (1979) *J. Am. Chem. Soc. 101*, 765−766.
Momenteau, M., & Reed, C. A. (1994) *Chem. Rev. 94*, 659−698.
Olson, J. S., Matthews, A. J., Rohlfs, R. J., Springer, B. A., Egeberg, K. A., Sligar, S. G., Tame, J., Renaud, J.-P., & Nagai, K. (1988) *Nature 336*, 265−266.
Quinn, R., Mercer-Smith, J., Burstyn, J. N., & Valentine, J. S. (1984) *J. Am. Chem. Soc. 106*, 4136−4144.
Rougee, M., & Brault, D. (1975) *Biochemistry 14*, 4100−4106.
Shiro, Y., Iizuka, T., Marubayashi, K., Ogura, T., Kitagawa, T., Balasubramanian, S., & Boxer, S. G. (1994) *Biochemistry 33*, 14986−14992.
Shulman, R. G., Wuthrich, K., Yamane, T., Patel, D. J., & Blumberg, W. E. (1970) *J. Mol. Biol. 53*, 143−157.
Smerdon, S. J., Krzywda, S., Wilkinson, A. J., Brantley, R. E., Jr., Carver, T. E., Hargrove, M. S., & Olson, J. S. (1993) *Biochemistry 32*, 5132−5138.
Springer, B. A., Sligar, S. G., Olson, J. S., & Phillips, G. N., Jr. (1994) *Chem. Rev. 94*, 699−714.
Takano, T. (1977) *J. Mol. Biol. 110*, 537−568.
Tetreau, C., Lavalette, D., Momenteau, M., Fischer, J., & Weiss, R. (1994) *J. Am. Chem. Soc. 116*, 11840−11848.
Theriault, Y., Pochapsky, T. C., Dalvit, C., Chiu, M. L., Sligar, S. G., & Wright, P. E. (1994) *J. Biomol. NMR 4*, 491−504.
Traylor, T. G., & Traylor, P. S. (1982) *Ann. Rev. Biophys. Bioeng. 11*, 105−127.
Traylor, T. G., & Popovitz-Biro, R. (1988) *J. Am. Chem. Soc. 110*, 239−243.
Traylor, T. G., Campbell, D., Sharma, V., & Geibel, J. (1979) *J. Am. Chem. Soc. 101*, 5376−5383.

BI952625T